GTPase assay. GTPase assays were performed as described[13]. Briefly, Ha-Ras (7 μl 1 μM Ha-Ras in 20 mM HEPES, pH 7.3, 2 mM DTT, 1 mg ml^{-1} BSA) was incubated for 5 min at 25 °C with [γ-^{32}P]GTP (6,000 Ci mmol^{-1}, NEN; 7 μl 0.1 μM diluted in 20 mM HEPES, pH 7.3, 2 mM DTT, 1 mM EDTA). [γ-^{32}P]GTP loading was stopped by the addition of 126 μl 20 mM HEPES, pH 7.3, 2 mM $MgCl_2$, 2 mM DTT. For each GTPase assay, 5 μl [γ-^{32}P]GTP-bound Ha-Ras was incubated for indicated times in the absence or presence of equal volumes of 1 nM Gap1^m in 20 mM HEPES, pH 7.3, 2 mM $MgCl_2$, 2 mM DTT, 100 μM GTP, 1 mg ml^{-1} BSA at 25 °C. In some reactions, certain concentrations of G proteins were included in the reactions. Measurement of free $^{32}P_i$ released from GTP hydrolysis was performed as described[26]. Briefly, unreacted GTP was precipitated by the addition of 260 μl acid-washed Norit-charcoal (5% in 20 mM phosphoric acid). After centrifugation (10 min), 100 μl the supernatant was analysed for free $^{32}P_i$ by scintillation counting.

Detection of activated Ras. The assay for the interaction of activated Ras with the GST-fusion protein containing the Ras-binding domain (RBD) of Raf-1 was performed as described[16]. COS-7 cells or MEG-01 cells, untransfected or transfected with Gα12 plasmid DNA, were grown for 48 h and then starved for 18 h. 3 μM U46619 was added for 10 min before the addition of 50 nM EGF for 5 min. Whole-cell extracts were prepared. Activated Ras-GTP was precipitated with 20 μl glutathione–agarose beads with GST–RBD fusion protein (~10 μg). After 12% SDS–PAGE, Ras was detected with anti-Ras antibodies.

Received 22 June; accepted 13 August 1998.

1. Gilman, A. G proteins: transducers of receptor-generated signals. *Annu. Rev. Biochem.* **56,** 615–649 (1987).
2. Bourne, H. R., Sanders, D. A. & McCormick, F. The GTPase superfamily: a conserved switch for diverse cell functions. *Nature* **348,** 125–132 (1990).
3. Simon, M. I., Strathmann, M. P. & Gautum, N. Diversity of G proteins in signal transduction. *Science* **252,** 802–808 (1991).
4. Clapham, D. E. & Neer, E. J. G protein βγ subunits. *Annu. Rev. Pharmacol. Toxicol.* **37,** 167–203 (1997).
5. Strathmann, M. P. & Simon, M. I. Gα12 and Gα13 subunits define a fourth class of G protein α subunits. *Proc. Natl Acad. Sci. USA* **88,** 5582–5586 (1991).
6. Dhanasekaran, N. & Dermott, J. M. Signaling by the G12 class of G proteins. *Cell. Signal.* **8,** 235–245 (1996).
7. Bence, K., Ma, W., Kozasa, T. & Huang, X.-Y. Direct stimulation of Bruton's tyrosine kinase by Gq-protein α-subunit. *Nature* **389,** 296–299 (1997).
8. Vihinen, M. *et al.* BTKbase: a database of XLA-causing mutations. *Immunol. Today* **16,** 460–465 (1995).
9. Vihinen, M., Nilsson, L. & Smith, C. I. E. Tec homology (TH) adjacent to the PH domain. *FEBS Lett.* **350,** 263–265 (1994).
10. Maekawa, M., Nakamura, S. & Hattori, S. Purification of a novel ras GTPase-activating protein from rat brain. *J. Biol. Chem.* **268,** 22948–22952 (1993).
11. Maekawa, M. *et al.* A novel mammalian Ras GTPase-activating protein which has phospholipid-binding and Btk homology regions. *Mol. Cell. Biol.* **14,** 6879–6885 (1994).
12. Gaul, U., Mardon, G. & Rubin, G. M. A putative Ras GTPase activating protein acts as a negative regulator of signaling by the Sevenless receptor tyrosine kinase. *Cell* **68,** 1007–1019 (1992).
13. Cullen, P. J. *et al.* Identification of a specific Ins(1,3,4,5)P_4-binding protein as a member of the GAP1 family. *Nature* **376,** 527–530 (1995).
14. Yamamoto, T., Matsui, T., Nakafuku, M., Iwamatsu, A. & Kaibuchi, K. A novel GTPase-activating protein for R-Ras. *J. Biol. Chem.* **270,** 30557–30561 (1995).
15. Voyno-Yasenetskaya, T. A., Faure, M. P., Ahn, N. G. & Bourne, H. R. Gα12 and Gα13 regulate extracellular signal-regulated kinase and c-Jun kinase pathways by different mechanisms in COS-7 cells. *J. Biol. Chem.* **271,** 21081–21087 (1996).
16. Taylor, S. J. & Shalloway, D. Cell cycle-dependent activation of Ras. *Curr. Biol.* **6,** 1621–1627 (1996).
17. Offermanns, S., Laugwitz, K.-L., Spicher, K. & Schultz, G. G proteins of the G12 family are activated via thromboxane A2 and thrombin receptors in human platelets. *Proc. Natl Acad. Sci. USA* **91,** 504–508 (1994).
18. Harhammer, R. *et al.* Distinct biochemical properties of the native members of the G12 G-protein subfamily. *Biochem. J.* **319,** 165–171 (1996).
19. Hirata, M. *et al.* Cloning and expression of cDNA for a human thromboxane A_2 receptor. *Nature* **349,** 617–620 (1991).
20. McCormick, F. Activators and effectors of ras p21 proteins. *Curr. Opin. Genet. Dev.* **4,** 71–76 (1994).
21. Kozasa, T. & Gilman, A. G. Purification of recombinant G proteins from Sf9 cells by hexahistidine tagging of associated subunits. *J. Biol. Chem.* **270,** 1734–1741 (1995).
22. Wan, Y., Kurosaki, T. & Huang, X.-Y. Tyrosine kinases in activation of the MAP kinase cascade by G-protein-coupled receptors. *Nature* **380,** 541–544 (1996).
23. Wan, Y. *et al.* Genetic evidence for a tyrosine kinase cascade preceding the mitogen-activated protein kinase cascade in vertebrate G protein signalling. *J. Biol. Chem.* **272,** 17209–17215 (1997).
24. Langhans-Rajasekaran, S. A., Wan, Y. & Huang, X.-Y. Activation of Tsk and Btk tyrosine kinases by G protein βγ subunits. *Proc. Natl Acad. Sci. USA* **92,** 8601–8605 (1995).
25. Zhang, J. J. *et al.* Two contact regions between Stat1 and CBP/p300 in interferon γ signaling. *Proc. Natl Acad. Sci. USA* **93,** 15092–15096 (1996).
26. Schwer, B. & Guthrie, C. PRP16 is an RNA-dependent ATPase that interacts transiently with the spliceosome. *Nature* **349,** 494–499 (1991).

Acknowledgements. We thank S. Taylor and D. Shalloway for the pGEX-RBD plasmid; M. Liu and M. Simon for the Gα12 plasmid; and M. Gershengorn, L. Levin, W. Lowry and T. Maack for reading the manuscript. Some of the Sf9 cells were cultured in the National Cell Culture Center. This work was supported by grants from the NIH, the NSF, and the American Heart Association. X.-Y.H. is a Beatrice F. Parvin Investigator of the American Heart Association New York City affiliate.

Correspondence and requests for materials should be addressed to X.-Y.H. (e-mail: xyhuang@mail.med.cornell.edu).

Direction determination in the minus-end-directed kinesin motor ncd

Elena P. Sablin*, Ryan B. Case*, Shirleko C. Dai*, Cynthia L. Hart*†, Aaron Ruby*, Ronald D. Vale*† & Robert J. Fletterick*

* *Departments of Biochemistry/Biophysics and Pharmacology and* † *Howard Hughes Medical Institute, University of California, San Francisco, California 94143, USA*

Motor proteins of the kinesin superfamily transport intracellular cargo along microtubules. Although different kinesin proteins share 30–50% amino-acid identity in their motor catalytic cores, some move to the plus end of microtubules whereas others travel in the opposite direction[1,2]. Crystal structures of the catalytic cores of conventional kinesin (a plus-end-directed motor involved in organelle transport) and ncd (a minus-end-directed motor involved in chromosome segregation) are nearly identical[3,4]; therefore, the structural basis for their opposite directions of movement is unknown. Here we show that the ncd 'neck', made up of 13 class-specific residues next to the superfamily-conserved catalytic core, is essential for minus-end-directed motility, as mutagenesis of these neck residues reverses the direction of ncd motion. By solving the 2.5 Å structure of a functional ncd dimer, we show that the ncd neck (a coiled-coil) differs from the corresponding region in the kinesin neck (an interrupted β-strand)[5,6], although both necks interact with similar elements in the catalytic cores. The distinct neck architectures also confer different symmetries to the ncd and kinesin dimers and position these motors with appropriate directional bias on the microtubule.

We determined the structure of an ncd homodimer (E281–K700, refs 7, 8; Fig. 1a, b) in a complex with Mg-ADP by using molecular-replacement methods (Table 1). The model of the ncd homodimer includes 740 amino-acid residues (amino acids (aa) 303–672 from each chain). The motor heads are connected through their 'necks', 13 residues that precede the first β-strand of the ncd catalytic core and are defined by high conservation among only the carboxy-terminal motor proteins of the kinesin superfamily (those kinesin proteins with motor domains at their C-terminal ends)[2] (Fig. 1a). The neck is entirely helical and partners symmetrically in the dimer to form a parallel coiled-coil (Fig. 1b). The conserved neck connects to the less conserved coiled-coil 'stalk' domain without any intervening loops. The coiled-coil helices of the neck are connected to the motor heads in each monomer through an abrupt turn that contains the conserved residue G347 at its apex. The structure of

Table 1 Data collection and model building and refinement

Space group: $P6_122$	
$a = 123.0$ Å, $b = 123.0$ Å, $c = 121.1$ Å	
Data collection	
Resolution (Å)	2.5
R_{sym} (%)	6.8
Unique reflections	18,795
Observed reflections	190,358
Completeness (%)	98.6
Refinement (20.0–2.5 Å)	
R_{cyst} (%)	22.6
R_{free} (%)	27.0
r.m.s. bond length (Å)	0.007
r.m.s. bond angle (degrees)	1.44
Average *B*-factor (Å^2)	23.5

r.m.s., root mean square.

each catalytic core is unchanged from the previously determined structure of the ncd monomer catalytic core[4]. An exception is loop L11 (Fig. 1b), which was possibly ordered by crystal packing in the monomer, but is disordered in the dimer structure.

The ncd dimer structure has two-fold symmetry, which is set by the coiled-coil domain. The two-fold symmetry of the ncd dimer seen in the crystal structure also exists in solution, as confirmed by low-angle X-ray scattering of the ncd–ADP complex (R. Mendelson, manuscript in preparation). However, the symmetrical structure of the ncd dimer must represent only one state of the motor during its mechanochemical cycle—the microtubule-dissociated ADP-bound state. Electron microscopic images of the ncd dimer bound to microtubules show that the two motor heads, even though they are still closely apposed as in the crystal structure, are not related by two-fold symmetry[9–11]. Therefore, a symmetry-breaking conformational change in the ncd dimer must be associated with binding of the motor to the microtubule and the subsequent release of ADP from the microtubule-bound head. The rotation of one head in the dimer crystal structure by ~25° about the two-fold axis could explain the position of the detached head in the cryo-electron microscopic images.

The neck and stalk coiled-coil domains interact with the catalytic core through an extensive network of interactions which creates a continuous interface of ~690 Å^2. The interacting core residues cluster mainly in the C-terminal part of helix α1 and loops L6, L10 and L13 (Fig. 2a, b). Six of the residues on ncd's catalytic core that form the interfacial surface are conserved only among the C-terminal, minus-end-directed kinesin motors (Q420, S421, D424, G472, W473 and K640)[4]. However, the residue Y426 is conserved throughout the kinesin superfamily[4] (it is equivalent to Y77 in human conventional kinesin). Six amino acids on the complementary interface of the ncd neck region (R335, K336, H339, N340, D344 and R346) are highly conserved among the C-terminal kinesin motors[2].

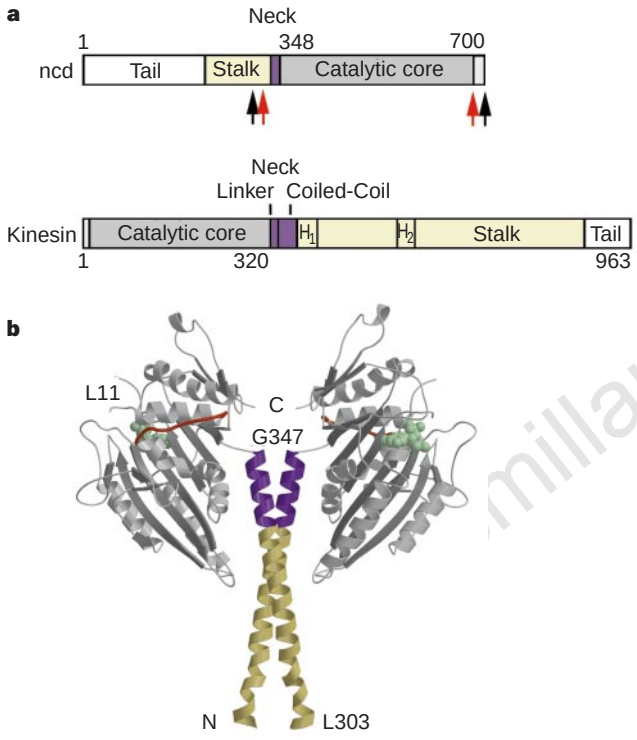

Figure 1 Structure of the ncd dimer. **a**, Domain organization of ncd and kinesin homodimers. The polypeptide chain of the monomer is organized into four domains (right to left, C to N terminus, in ncd; left to right in kinesin). First, there is a globular catalytic core (grey), which contains the ATP- and microtubule-binding sites and is conserved throughout the kinesin superfamily. The ncd catalytic core is about 40% identical in sequence to kinesin's catalytic core but, in contrast to in kinesin, it is located at the C terminus of the ncd polypeptide chain. Second, there is a 'neck' region (purple), which is adjacent to the catalytic core and is defined by class-specific sequence conservation[12]. The neck of ncd contains 13 class-conserved amino acids (R335–G347) that precede the first β-strand of the catalytic core. Kinesin's conserved neck (~35 residues) emerges from the C terminus of the catalytic core and consists of two distinct regions. The first ten residues, termed the 'neck linker', are highly conserved among all plus-end-directed motors and interact with the catalytic core. The subsequent region forms a coiled-coil ('neck coiled-coil'), does not interact with the core, and is conserved selectively among the conventional kinesin subfamily[12]. Third, there is an α-helical 'stalk' domain (yellow) that enhances dimer formation through an extended coiled-coil. $H_1$and H_2 indicate flexible hinge regions. finally, there is a small C-terminal 'tail' or attachment domain (white). The black and red arrows delineate the characterized ncd fragment and the visible part of the structure, respectively. **b**, View perpendicular to the dyad axis showing the course of the polypeptide chains of ncd; the dimer has dimensions of ~95 × 105 × 65 Å, with the two catalytic cores (heads) positioned 45 Å from each other. The colouring scheme is consistent with **a**. ADP is shown in the active site in green. One of the important secondary-structure elements involved in microtubule-binding (loop L12) is shown in orange.

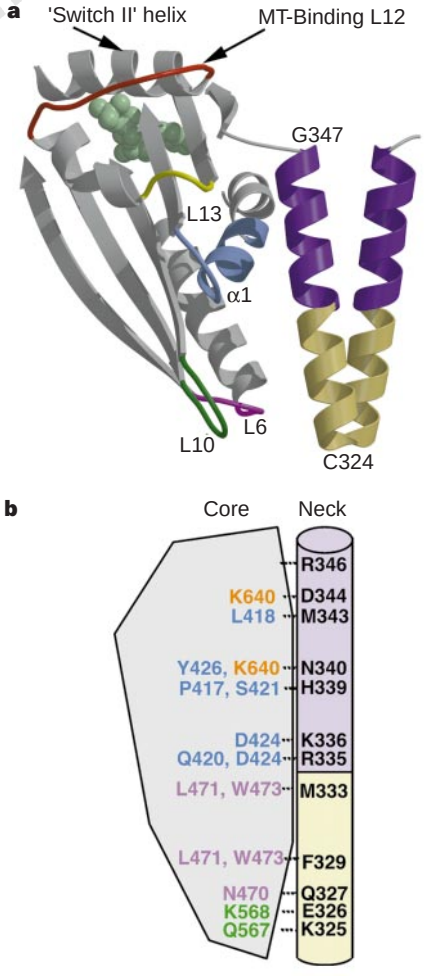

Figure 2 Architecture of the ncd neck–core interface. **a**, Interactions of the neck with the motor heads: the neck is shown in purple; regions of the core that contact the neck are shown in blue (α1), magenta (L6), green (L10) and yellow (L13); and the stalk domain is golden. Loop L13 is next to the predicted microtubule (MT)-binding site of ncd (loop L12 and helix α5). Bound ADP is shown as green spheres. **b**, The interdomain contacts; the colouring scheme for the interacting residues in the core is consistent with **a**.

Table 2 Microtubule gliding velocities of ncd mutants

Construct	Motor direction	Velocity (% wild-type)
Wild-type	Minus	100 ± 5
E567A/K568A	Minus	99 ± 11
H339A/N340A	Minus	76 ± 11
G636A/G637A	Minus	79 ± 7
Y426A	Minus	57 ± 7
Q420A/S421A	Minus	44 ± 14
R335A/K336A	Minus	49 ± 9
K640A	Minus	34 ± 0.2
Q420A/S421A/Y426A	Minus	10 ± 1
NCD-ran12 (aa335 RKE LHN TVMDLR aa346 to ESGAKQGE K GES)	Plus	2 ± 0.3

The gliding velocity of wild-type ncd–GFP was $8.4 \pm 0.4\,\mu m\,min^{-1}$. Values are the mean ± s.d. of the average velocities obtained from two to three independent protein preparations (50 microtubules per preparation). The affinity of ncd-ran12 for microtubules in the motility assay was lower than that of wild-type, and fewer microtubules were observed on the ncd-ran12 surface.

To study the function of conserved residues in the ncd neck–core interface, we prepared nine mutants and tested their motility (Table 2). The most drastic mutation replaced 12 neck residues (aa 335–346) with random, hydrophilic residues (ESGAKQGEKGES; named ncd-ran12), which should completely disrupt the neck–core interaction and the coiled-coil architecture of the ncd neck. Most of the mutations had small effects on motility (less than twofold change). However, mutant K640A and the triple mutant Q420A/S421A/Y426A exhibited 3- and 10-fold, respectively, lower microtubule gliding velocities (minus-end-directed) than wild-type ncd. Surprisingly, ncd-ran12 moved slowly (at $0.16\,\mu m\,min^{-1}$) towards the microtubule plus end, that is, in the opposite direction to the wild-type ncd motor. As ncd-ran12 lacks its conserved neck, its motility may be generated through a small plus-end-directed conformational change associated with the catalytic core, as may also occur for a similar neck-replaced kinesin mutant (R. Case *et al.*, manuscript in preparation).

Although the Q420A/S421A/Y426A and ncd-ran12 mutants generated slow motility, their ATPase turnover was nearly normal, indicating that nucleotide hydrolysis had become uncoupled from motility (k_{cat} values of 1.5 ± 0.1, 0.9 ± 0.2 and 1.4 ± 0.2 ATP molecules hydrolysed per head per second by wild-type ncd, Q420A/S421A/Y426A and ncd-ran12 respectively; mean ± s.d. of values from 2–3 protein preparations). These mutants also exhibited lower affinity for microtubules, as reflected by their elevated K_m (microtubules) for ATPase activation (1.0 ± 0.1, 1.7 ± 0.7, 19.4 ± 7.4 μM tubulin dimer for wild-type ncd, Q420A/S421A/Y426A and ncd-ran12, respectively). These results indicate that ncd motor activity can be uncoupled from ATP turnover by mutating conserved residues at the neck–core interface and that an intact neck is essential for generating minus-end-directed motion.

There are major differences between the dimeric ncd and conventional kinesin[5] crystal structures that may be relevant to understanding their opposite directions of motion (Fig. 3). First, the arrangements of the heads differ in the two motor dimers. The kinesin heads do not show two-fold symmetry but are related by a ~120° rotation and also are positioned further apart from each other than the heads of ncd. The different symmetries of the kinesin and ncd dimers appear to be determined by their distinct neck architectures. In contrast to the continuous coiled-coil of the ncd neck, the kinesin neck consists of two short β-strands (β9 and β10; termed the neck linker) followed by the coiled-coil helix α7 (neck coiled-coil), all of which are connected by short loops[5] (Figs 1 and 3). According to the crystal structures, if the bound ncd and kinesin heads are positioned similarly on a microtubule, as indicated by cryo-electron microscopic experiments[12], then the unbound kinesin head would point towards the microtubule plus end, whereas the unbound ncd head would be tilted towards the minus end (Fig. 3). This analysis indicates that the different symmetries of the ncd and kinesin heads in dimeric motors position the detached heads in the direction of motor movement. The different positioning of the two heads by their necks, which is consistent with cryo-electron microscopic studies of microtubule-bound ncd and kinesin dimers[9,10], should contribute to the opposite direction of movement of these two motors.

Despite their different sequences and structures, the ncd and kinesin necks both follow the same path and interact with the same secondary-structure elements in the catalytic core (mainly the α1/β3 turn and loop L13). This similarity was not expected, because the helical neck of ncd emerges before the amino terminus of the catalytic core, whereas the kinesin neck follows the C terminus of the core. In both cases, the neck–core contacts are near the main microtubule-binding loop, L12 (refs 11, 13), and the 'switch II' helix α4 (Fig. 2a), which are thought to change conformation during the nucleotidase cycle[4]. Two major predictions can be made on the basis of this observation. First, the catalytic core could convey information about its nucleotide- and microtubule-binding state in a similar manner (through α1 and L13) to the necks of both motors. However, the necks, because of their different architectures, must respond and transmit this information to the unattached, partner heads differently, so that they can move in opposite directions along the microtubule. Second, the similar core–neck communication pathway in both motors could explain the co-functioning of the kinesin neck with the ncd catalytic core in chimaeric proteins[14,15].

Our structural and motility data indicate that the helical neck domain of ncd, with its sophisticated interactions with the core, is necessary for generating minus-end-directed motion. How does the ncd neck function in the force-generating cycle? Although the

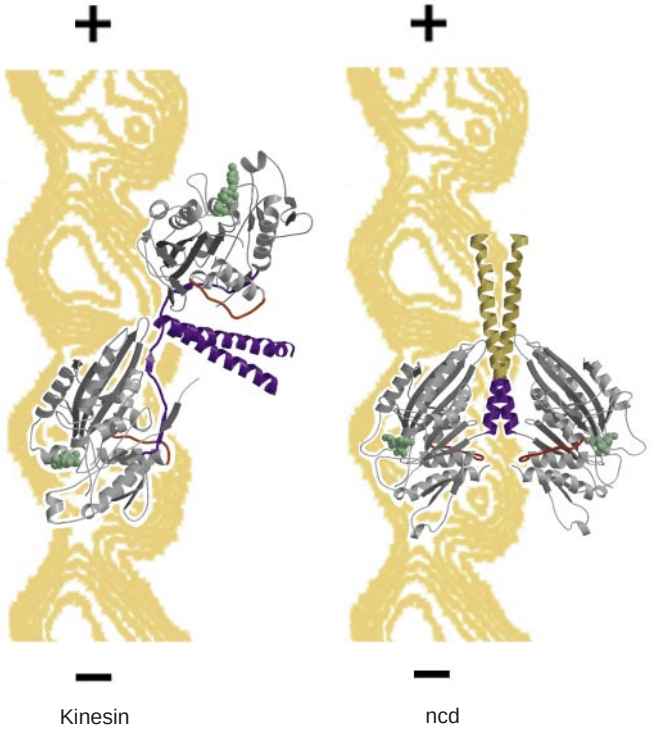

Figure 3 Model showing the ncd and kinesin dimer structures docked onto a tubulin protofilament. The colouring scheme for the parts of the kinesin and ncd dimers is consistent with Fig. 1. The bound ncd and kinesin heads are positioned similarly, with loop L12 (red) docked onto the tubulin (background). Because of the distinct architectures of the kinesin and ncd necks, the unbound kinesin head points towards the plus end, whereas the unbound ncd head is tilted towards the minus end of the protofilament.

helical structure of the neck may be stabilized by its specific interactions with the catalytic core in the ncd-dimer–ADP complex, the neck may be able to adopt other conformations during the enzymatic cycle. In support of this idea, predictive analysis indicates that the ncd neck residues (R335–G347) are not expected to form either a stable α-helix (PHD program)[16] or a coiled-coil (COILS program)[17], and a synthetic peptide corresponding to the ncd neck (L328–R348) is not helical in solution (B. Tripet and R. S. Hodges; and T. Shimizu, M. Itoh, H. Morii and M. Tanokura, personal communications). Moreover, the neck is disordered and not bound to the core in the ncd monomer structure[4]. The polar character of the residues at the neck–core interface also indicates that this region is designed to be dynamic. We propose that the ncd force-generating mechanism includes a conformational change of the neck, possibly involving a partial or complete loss of its α-helical structure. Conformational transitions of the neck could be initiated from the nearby nucleotide-binding and microtubule-binding sites (through the switch II and L12 regions, respectively) and transmitted through the neck–core interface. The net result of this conformational transition would be expected to produce a force vector directed towards the microtubule minus end and, possibly, a torque, which has been seen in ncd motility assays[18]. In contrast, the kinesin neck appears to amplify motion towards the microtubule plus end (R. Case *et al.*, manuscript in preparation). In the ncd and kinesin dimers, the oppositely directed actions of the neck in the microtubule-bound head would then be further amplified by the detached partner heads, which are positioned with appropriate directional bias in the two motors. □

Methods

Expression, purification and crystallization of the ncd dimer. A DNA fragment encoding residues E281–K700 of the ncd motor protein[7,8] was synthesized by the polymerase chain reaction (PCR) and cloned into the translation vector pHB40P. The recombinant plasmid was transformed into BL21(DE3)pLysE host cells (Novagen) for expression. Cells were grown at 24 °C in LB media supplemented with ampicillin (0.1 mg ml^{-1}) and induced by addition of 0.2 mM of isopropyl-β-D-thiogalactoside (IPTG) for 8 h. Packed, induced cells were resuspended in PB buffer (10 mM PIPES, pH 7.2, 100 mM NaCl, 2 mM $MgCl_2$, 1 mM EGTA, 1 mM dithiothreitol (DTT), and protease inhibitors) with 0.1 mg ml^{-1} DNAase 1, and lysed using a French pressure cell press (American Instrument). The supernatant from a 60,000*g* centrifugation for 1 h was loaded onto a SP–Sepharose FF (Pharmacia) column equilibrated in PB. A linear NaCl gradient (0.1–0.3 M) was used to elute the ncd, and the pooled fractions were dialysed against TB buffer (10 mM Tris-HCl, pH 7.4, 80 mM NaCl, 2 mM $MgCl_2$, 1 mM DTT and protease inhibitors) and loaded onto a MonoQ Hr10/10 column (Pharmacia) equilibrated in TB. A linear NaCl gradient (0.1–0.3 M) was applied to elute ncd, which was then concentrated to ~20 mg ml^{-1} using a Centricon-30 (Amicon) and used fresh for crystallization. The purified protein showed a microtubule-activated ATPase activity of 0.5 ATP molecules per head per second. Crystals were obtained by vapour diffusion using 20 μl sitting drops. The mother liquor contained protein at about 20 mg ml^{-1}, 2 mM ADP, 10 mM $MgCl_2$, 100 mM NaCl, 700 mM Li_2SO_4. 1 mM EGTA and 1 mM DTT in 20 mM HEPES, pH 7.5. The reservoir was 1.4 M Li_2SO_4, 10 mM $MgCl_2$, 1 mM EGTA and 1 mM DTT in 20 mM HEPES, pH 7.5. Crystals appeared after 2 weeks at +4 °C, and were of the hexagonal space group $P6_122$, with one ncd monomer plus bound Mg-ADP per asymmetric unit.

Data collecting, model building and refinement. X-ray diffraction data to 2.5 Å resolution were measured at −170 °C using 30% (*v/v*) glycerol in precipitant solution as a cryosolvent. The data were collected at Stanford Synchrotron Radiation Laboratory beamline 7-1 ($\lambda = 1.08$ Å), integrated using DENZO and scaled with SCALEPACK (Z. Otwinowski and W. Minor). The structure of the ncd dimer was determined to 2.5 Å by molecular replacement (AMoRe) using atomic coordinates for the ncd monomer (residues R335–K700)[4]. An electron-density map based on coefficients $2F_o - F_c$ was calculated from the phases of the initial model. The additional parts of the structure were built and placed in visible density using the program O (T. A. Jones and M. Kjeldgaard). Later stages of model building included conjugate gradient minimization and refinement by simulated annealing using X-PLOR[19]. The entire structure was checked and rebuilt using annealed omit maps. The current atomic model includes 740 amino-acid residues together with 2 Mg-ADP complexes, 54 water molecules and 4 sulphate anions. The final maps based on the refined coordinates, contain electron density for amino-acid residues from L303 to M672. Electron density is missing for the N-terminal amino-acid residues 281–302, loop L11 (aa 588–596) and C-terminal residues 673–700.

Mutagenesis. Site-directed mutagenesis using Stratagene's QuikChange protocol was done in a previously characterized ncd–green fluorescent protein (GFP) construct which consisted of a His_6 tag at the N terminus of GFP, a 2-amino-acid Gly–Thr linker (*Kpn1* site) at the C terminus of GFP, followed by ncd residues 236–700 (refs 7, 15). The sequences of all constructs were verified. Protein was expressed in bacteria, applied to Ni-NTA resin (Qiagen), and further purified on a mono-S or high trap-SP column (Pharmacia) as described[15]. Protein purity was in the range 50–85%, with most contaminants representing degradation products. Protein concentration was measured as described[13]. Proteins were frozen (10% sucrose added) and stored in liquid nitrogen.

Microtubule-stimulated ncd ATPase was measured in 15 mM NaMOPS (pH 7), 3 mM NaCl, 2 mM $MgCl_2$, 1 mM EGTA, 1 mM DTT, 1 mM ATP and 10 μM paclitaxel using a malachite green assay[20]. Gliding assays for ncd–GFP were performed using rhodamine-labelled microtubules and fluorescence microscopy as described[15]. For slow-moving proteins (<1 μm min^{-1}), we used polarity-marked, rhodamine-labelled microtubules[21] to ensure that all motion was unidirectional and that stage drift did not account for the motion; the illumination was shuttered to reduce damage from free radicals. We quantified 50 microtubule gliding speeds and directionalities for each protein preparation.

Received 14 May; accepted 2 September 1998.

1. Hirokawa, N. Kinesin and dynein superfamily proteins and the mechanism of organelle transport. *Science* **279,** 519–526 (1998).
2. Vale, R. D. & Fletterick, R. J. The design plan of kinesin motors. *Annu. Rev. Cell Dev. Biol.* **13,** 745–777 (1997).
3. Kull, F. J., Sablin, E. P., Lau, R., Fletterick, R. J. & Vale, R. D. Crystal structure of the kinesin motor domain reveals a structural similarity to myosin. *Nature* **380,** 555–559 (1996).
4. Sablin, E. P., Kull, F. J., Cooke, R., Vale, R. D. & Fletterick, R. J. Crystal structure of the motor domain of the kinesin-related motor ncd. *Nature* **380,** 555–559 (1996).
5. Kozielski, F. *et al.* The crystal structure of dimeric kinesin and implications for microtubule-dependent motility. *Cell* **91,** 985–994 (1997).
6. Sack, S. *et al.* X-ray structure of motor and neck domains from rat brain kinesin. *Biochemistry* **36,** 16155–16165 (1997).
7. McDonald, H. B. & Goldstein, L. S. Identification and characterization of a gene encoding a kinesin-like protein in *Drosophila*. *Cell* **61,** 991–1000 (1990).
8. Endow, S. A., Henikoff, S. & Soler, N. L. Mediation of meiotic and early mitotic chromosome segregation in *Drosophila* by a protein related to kinesin. *Nature* **345,** 81–83 (1990).
9. Hirose, K., Lockhard, A., Cross, R. A. & Amos, L. A. Three-dimensional cryoelectron microscopy of dimeric kinesin and ncd motor domains on microtubules. *Proc. Natl Acad. Sci. USA* **93,** 9539–9544 (1996).
10. Arnal, I., Metoz, F., DeBonis, S. & Wade, R. H. Three-dimensional structure of functional motor proteins on microtubules. *Curr. Biol.* **6,** 1265–1270 (1996).
11. Sosa, H. *et al.* A model for the microtubule-Ncd motor protein complex obtained by cryo-electron microscopy and image analysis. *Cell* **90,** 217–224 (1997).
12. Amos, L. A. & Hirose, K. The structure of microtubule–motor complexes. *Curr. Opin. Cell Biol.* **9,** 4–11 (1997).
13. Woehlke, G. *et al.* Microtubule interaction site of the kinesin motor. *Cell* **90,** 207–216 (1997).
14. Henningsen, U. & Schliwa, M. Reversal in the direction of movement of a molecular motor. *Nature* **389,** 93–96 (1997).
15. Case, R. B., Pierce, D. W., Hom-Booher, N., Hart, C. L. & Vale, R. D. The directional preference of kinesin motors is specified by an element outside of the motor catalytic domain. *Cell* **90,** 959–966 (1997).
16. Rost, B. & Sander, C. PHD: predicting one-dimensional protein structure by profile based neural networks. *Methods Enzymol.* **266,** 525–539 (1996).
17. Lupas, A., Van Dyke, M. & Stock, J. Predicting coiled coils from protein sequences. *Science* **252,** 1162–1164 (1991).
18. Walker, R. A., Salmon, E. D. & Endow, S. A. The *Drosophila* claret segregation protein is a minus-end directed motor molecule. *Nature* **347,** 780–782 (1990).
19. Brunger, A. T. *X-PLOR Version 3.1. A System for X-ray Crystallography and NMR* (Yale Univ. Press, New Haven, 1992).
20. Kodama, T., Fukui, K. & Kometani, K. The initial phosphate burst in ATP hydrolysis by myosin and subfragment 1 as studied by a modified Malachite Green method for determination of organic phosphate. *J. Biochem.* **99,** 1465–1472 (1986).
21. Hyman, A. A. Preparation of marked microtubules for the assay of the polarity of microtubule-based motors by fluorescence. *J. Cell Sci.* **Suppl. 14,** 125–127 (1991).

Acknowledgements. We thank M. Matuska for technical assistance, and J. Somoza and C. Sindelar for comments on manuscript. E.P.S. was supported by a postdoctoral fellowship from the Leukemia Society of America. This work was supported in part by a program project grant from the NIH.

Correspondence and requests for materials should be addressed to R.D.V. (e-mail: vale@phy.ucsf.edu). X-ray crystallographic coordinates have been deposited in the Protein Data Bank under accession numbers 2ncd and r2ncdsf.